Water Infiltration in Methylammonium Lead Iodide Perovskite: Fast and Inconspicuous.

Christian Müller[‡,†,⊥,§], Tobias Glaser[‡,⊥,§], Marcel Plogmeyer[⊥,§], Michael Sendner[⊥,§], Sebastian Döring[†], Artem A. Bakulin[+], Carlo Brzuska[#], Roland Scheer[#], Maxim S. Pshenichnikov[∩], Wolfgang Kowalsky[†,⊥,§], Annemarie Pucci[*,⊥,§,‖], and Robert Lovrinčić[*,†,§]

[†]Institut für Hochfrequenztechnik, TU Braunschweig, Schleinitzstr. 22, 38106 Braunschweig, Germany

[⊥]Kirchhoff-Institut für Physik, Universität Heidelberg, Im Neuenheimer Feld 227, 69120 Heidelberg, Germany

[§]InnovationLab, Speyerer Str. 4, Heidelberg, Germany

[+]Cavendish Laboratory, Cambridge University, J J Thomson Avenue, CB3 0HE Cambridge, United Kingdom

[#]Institut für Physik, Universität Halle-Wittenberg, von-Danckelmann Platz 3, 06099 Halle, Germany

[∩]Zernike Institute for Advanced Materials, University of Groningen, Nijenborgh 4, 9747 AG Groningen, The Netherlands

[‖]Centre for Advanced Materials, Universität Heidelberg, Im Neuenheimer Feld 225, 69120 Heidelberg, Germany

ABSTRACT: While the susceptibility of $CH_3NH_3PbI_3$ to water is well documented, water influence on device performance is not well understood. Herein we use infrared spectroscopy to show that water infiltration into $CH_3NH_3PbI_3$ occurs much faster and at much lower humidity than previously thought. We propose a molecular model where water molecules have a strong effect on the hydrogen bonding between the methylammonium cations and the Pb-I cage. Furthermore, the exposure of $CH_3NH_3PbI_3$ to ambient environment increases the photocurrent of films in lateral devices by more than one order of magnitude. The observed slow component in the photocurrent buildup indicates that the effect is associated with enhanced proton conduction when light is combined with water and oxygen exposure.

Introduction

The advent of hybrid organic inorganic perovskites[1], such as methylammonium lead iodide[2] ($CH_3NH_3PbI_3$, MAPbI), has led to an unprecedented revolution in photovoltaic research.[3–6] However, our understanding of physical/chemical processes in the material is trailing behind device performance progress.[7] As a consequence, the field is currently struggling with contradictory results reported on many basic properties, with hysteresis effects in photovoltaic performance being the most obvious example. Some groups connect it to ferroelectric phenomena[8,9], while others relate the effect to ionic migration[10,11] but without a consensus on the migrating species. Iodide[12], methyl ammonium[13], and hydrogen[14,15] have all been suggested as the primary mobile ions. Similarly, grain boundaries have been proposed as having both negligible[16] and beneficial[17] effects on charge separation, based on nominally identical Kelvin probe measurements. One possible explanation for these contradicting results is small and unappreciated variations in the fabrication processes. A clear candidate for such

unrecognized variations is the exposure to humidity. The strong impact of moisture on opto-electronic properties of MAPbI has been highlighted only very recently.[18–23] It was shown that exposure to small amounts of water during crystallization and annealing can improve performance of resulting devices.[19,24–26] Post-processing exposure to moderate humidity for minutes or hours can also improve the device performance[19], but exposure for days leads to a strong degradation[20]. Recent micro-Raman data suggest an interaction of water molecules with the organic cation at ambient conditions.[27] Prolonged exposure to high humidity results in the formation of the colorless hydrate $CH_3NH_3PbI_3 \cdot H_2O$ or $(CH_3NH_3)_4PbI_6 \cdot 2H_2O$, a process that was shown to be at least partially reversible,[28,29] and ultimately in complete decomposition of the material.[30]

Here, we show with infrared (IR) spectroscopy that water absorbs rapidly (on a seconds time scale) into MAPbI even at a relative humidity (RH) as low as 10% without changing light absorption in the visible range. The process is fully reversible by exposing the material to vacuum or nitrogen. The IR spectra allow us to propose a molecular model in which the water molecules remain separated rather than forming extended 3D hydrogen-bond networks, and their embedding has a strong influence on the hydrogen bonding between the methylammonium cations and the surrounding Pb-I cage. A peak area analysis suggests that at ambient conditions every other MAPbI unit cell is occupied by a water molecule. Furthermore, electrical characterizations of simple lateral devices show that the exposure to ambient environment increases the photocurrent by more than one order of magnitude. The slowest component of this increase of photocurrent appears on a time scale of minutes, which points to a possible role of absorbed water and oxygen in ionic conductivity or even photochemistry in MAPbI.

Experimental details

MAPbI film preparation. SiO_2 or substrates were cut and cleaned by sonication in acetone and isopropyl alcohol followed by drying in a N_2 stream. We used as received $PbCl_2$ (Sigma-Aldrich) and MAI, synthesized as reported elsewhere.[31] MAPbI thin films by co-evaporation of $PbCl_2$ and CH_3NH_3I in vacuum.[32] This method yields reproducible samples with high optical quality. The vacuum chamber was pumped down to 10^{-6} mbar. The MAI source was then slowly heated up until the chamber pressure rose to $1–2 \cdot 10^{-4}$ mbar (~120°C). Afterwards the PbCl source was heated up to reach an evaporation rate of 6 nm/min (~300°C). The as fabricated perovskite films were then transferred to a nitrogen filled glovebox and annealed for 45 minutes at 100°C (except the sample for Fig. 1 b which was not annealed). Ex-situ X-ray diffraction measurements on co-evaporated films showed only peaks corresponding to the perovskite structure and no traces of PbCl. Typical grain size of our films on Si is in the order of several 100 nm (see SI).

IR spectroscopy. The perovskite films were transferred to a Bruker Vertex 80v Fourier transform IR spectrometer in ambient air. Spectra were measured at normal incidence with the samples in vacuum (~2 mbar), under ambient conditions, and under nitrogen atmosphere with a controlled RH. RH was adjusted with a water bubbler setup. We used a DLaTGS (Figure 1, S8 and S9) or MCT (otherwise)

detector and non-polarized light. Spectral resolution was set to 4 cm^{-1} and all spectra are referenced to the spectrum of the bare Si-substrate with native oxide.

Electrical characterization. Gold (150 nm) electrodes with 200 µm spacing were evaporated on glass with titanium (7 nm) as adhesion layer (see Fig. S2). MAPbI was deposited on top via co-deposition as described above. The sample was mounted in a small vacuum chamber equipped with a turbo pump. The chamber was attached to a gas system that allowed controlled venting with the desired gas.
Electrical currents were measured with a Keithley 2636A sourcemeter. A solar simulator from LOT was used as light source for the photocurrent measurements. The light intensity was adjusted to 1 sun with the help of a calibrated Si solar cell.

Results

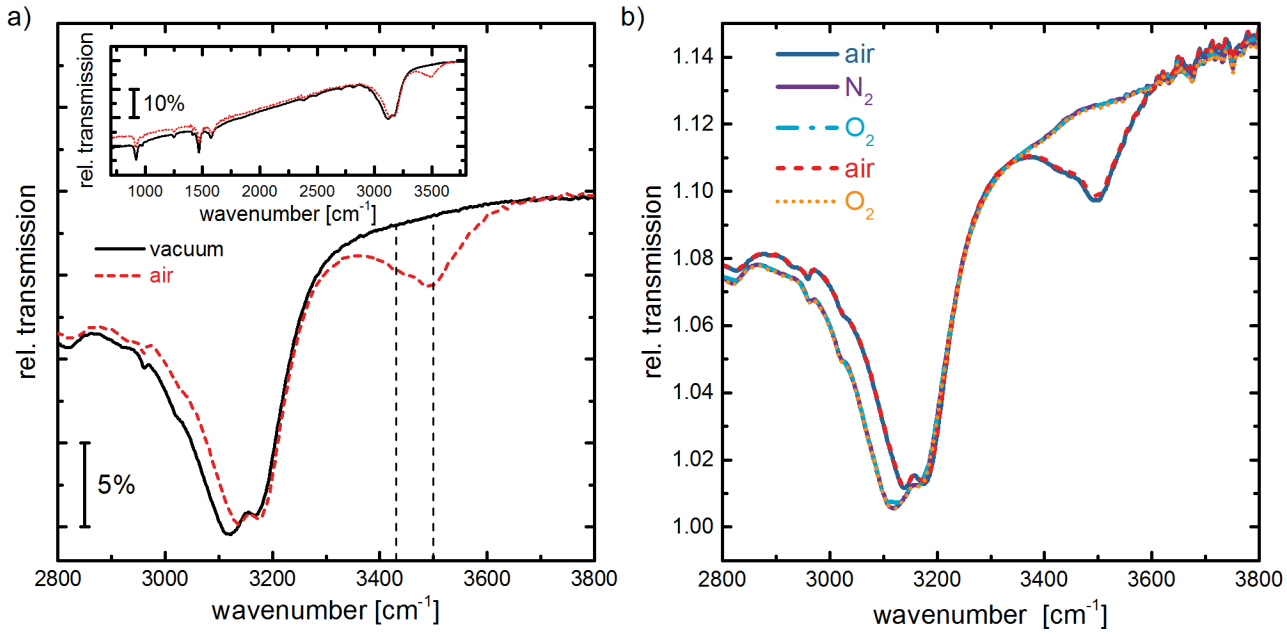

Figure 1. a) IR spectra of 300 nm thick MAPbI on a Si substrate measured in vacuum (3 mbar) and in ambient conditions (45% RH, 22°C). A strong peak at around 3500 cm^{-1} indicative of O-H stretch vibrations appears within less than 1 minute exposure to air. Dashed lines mark the positions of the O-H vibrations. Concurrently, the N-H stretch vibrations change. The process is fully reversible. The inset shows the complete mid-IR region of the spectra. b) IR spectra of 200 nm MAPbI on Si in different gas environments. The OH peaks and frequency shift of the NH peak are clearly seen in air, but disappear when the sample is exposed to dry nitrogen or oxygen. The reversibility is highlighted by repeated exposure to air (from the top to the bottom in the legend).

We have previously reported a detailed analysis of the mid IR spectrum[33] and ultrafast 2D-IR measurements[34] of MAPbI. Our mid-IR data have since been confirmed and expanded to the far IR theoretically[35] and experimentally.[36] Here, we focus on the change of the IR spectrum upon short and controlled exposure to ambient environment. Figure 1a shows the IR spectra of a 300 nm thick MAPbI film on Si measured in vacuum and right

after exposure to ambient conditions (~1 minute, limited by time necessary for conditions to stabilize). The doublet in the vacuum spectrum around 3150 cm^{-1} is assigned to symmetric (3120 cm^{-1}) and asymmetric (3170 cm^{-1}) NH_3^+ stretch vibrations, respectively.[33] Upon exposure to air the spectrum quickly (within seconds) changes: the symmetric N-H vibration reduces in strength, both NH stretches shift to higher frequencies, while a new broad peak around 3500 cm^{-1} arises. This additional peak is clearly attributed to OH stretch vibrations. We observed this effect for co-evaporated films with and without annealing and spin-coated films (see SI). Figure 2b shows that the process is reversible simply by exposing the film to dry environment.

We can draw several important conclusions from the IR spectra. First, the OH vibration consist of two distinct peaks (at 3430 cm^{-1} and 3500 cm^{-1}) typical for separated water molecules in solvents[37] or reversed micelles[38]. Hence, there is no or little bulk water with extended 3D hydrogen-bonded network in the sample which is readily identified by a broad featureless peak[39] around 3400 cm^{-1}. Second, the embedded water molecules form relatively strong hydrogen bonds because for weak hydrogen bonding the OH peaks would be situated above 3500 cm^{-1}.[37] The presence of two, symmetric and asymmetric, vibrations points towards both OH oscillators of water being in a similar environment – i.e. forming hydrogen bonds of similar strengths. Third, the water is not just adsorbed on the MAPbI surface, but infiltrates the material as mere surface adsorption would not cause the simultaneous change of the N-H stretch vibration. Fourth, the water molecules are embedded in such a way that they affect the hydrogen bonds between the NH_3^+ group and the iodide because the N-H stretch vibrations are known for their sensitivity to the strength of the interaction between the methylammonium and the iodide[33].

All these facts yield the following molecular-level picture of water embedment in the perovskite lattice. Water molecules affect the hydrogen bonds between MA and iodine ions by occupying the same unit cell of the crystal. Most probably, one of the NH groups forms a hydrogen bond with the oxygen of water while the water OH groups interact with the iodide ions. The observed shift and decrease of NH_3^+ symmetric stretching vibration is explained by the interaction of water's oxygen atom with one of the NH oscillators. This induces the change in NH stretching energy for one of the oscillators and converts the NH_3 vibrations to the NH_2 vibrations with higher frequency.

Water infiltration starts through defects and grain boundaries, as OH peak strength depends on the microstructure of the films (see SI). In particular, we observed no OH peaks for single MAPbI crystals in air (see SI). Next, water rapidly proceeds into the grains as adsorption on internal surfaces alone would not be able to shift the position of the N-H vibration. The total interaction energy of embedded water molecules is low so that water molecules stay mobile and are able to leave the crystal. This finding is also compatible with recent theoretical simulations of water infiltration in MAPbI.[22,40] Furthermore, Mosconi *et al*. showed with *ab initio* molecular dynamics calculations that water incorporation into MAPbI is possible without a significant change of the crystal structure.[40] To verify this conclusion, we performed additional X-ray diffraction measurements on MAPbI films in vacuum and air (see SI), and indeed observed no significant change of the lattice constants. Additionally, our optical absorption and photoluminescence measurements (see SI) show that the band gap does not change upon exposure to air, which is in good accordance with Mosconi *et al*.'s prediction of a widening of the band gap by only 0.05 eV for low water loads.

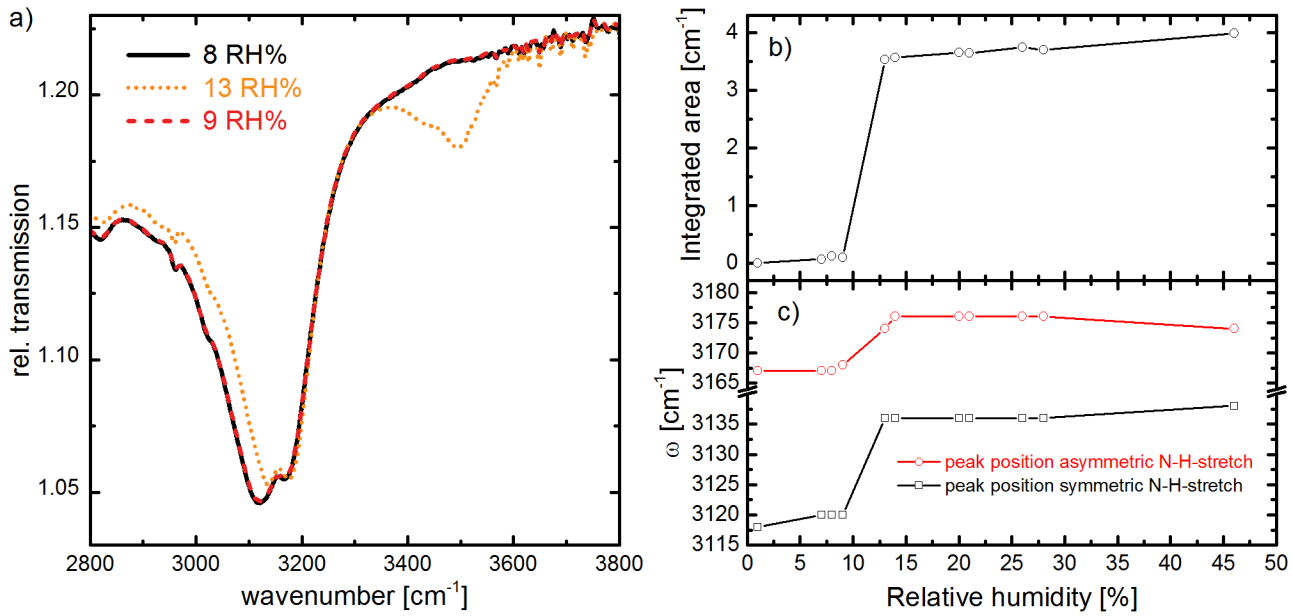

Figure 2. a) Relative transmittance of 300 nm MAPbI on a Si substrate measured in nitrogen atmosphere with varying relative humidity (RH) as indicated. b) Integrated area of the OH-stretching vibration mode in the range of 3360- 3600 cm^{-1} for the same film as function of RH. For the area calculations, the spectra have been corrected with a linear baseline and the spectrum in pure nitrogen atmosphere was subtracted from each spectrum. The uncertainty of RH is 5%. Symbol size corresponds to error bar along the y-axis. c) Peak positions of N-H stretch vibrations as a function of RH.

To investigate if the amount of absorbed water depends on RH, IR measurements were performed under controlled environment by exposing the samples to humidified N_2. Figure 2a shows the relative transmittance of 300 nm thick MAPbI on a Si substrate measured in nitrogen atmosphere with varying relative humidity as indicated. The spectra were taken directly after each other in the order 8 RH% - 13 RH% - 9 RH% as soon as the relative humidity stabilized (~1 minute). The OH peaks and concurrent shift of the NH vibration appear when the RH humidity is increased to 13 %, and disappear again at 9 % RH. Figure 2b shows the strength of the OH peaks as function of the RH of the surrounding N_2. We find no water at RH<10%, then a sudden increase at RH=10% with again little change up to 50% RH. Therefore, already at RH as low as ~10% almost every accessible site within the MAPbI sample is occupied with a water molecule. Figure 2c shows the concurrent shifts of the symmetric and asymmetric N-H stretch vibrations which show excellent correlation with the OH peak area thereby lending additional support to the proposed molecular-level picture.

The OH peak area can be furthermore used to estimate the amount of absorbed water molecules (see SI for details on calculation). We determined the imaginary part of the dielectric function for the hydrated film and relate the OH peak area to the density of OH oscillators via the sum rule.[41,42] Using an effective charge of 0.42e for the hydrogen atoms in water[43] and a dielectric constant of 5.0[33], we obtained an oscillator density of 4.1×10^{27} cm^{-3}. With two oscillators per water molecule and a unit cell volume[44] of 251.6×10^{-30} m^3, this corresponds to one water

molecule per every second unit cell. This value will change with the film morphology, as we found that the OH peak area changes depending on the processing (see SI).

The OH peak intensity does increase further (and the whole IR spectrum changes drastically) when the samples are exposed to water saturated environment and the optically transparent hydrate has formed. This process is only partially reversible as the films change their morphologies when the hydrated material is dried again (see SI).

Our finding of a strong water infiltration into MAPbI already at low RH has strong implications on our understanding of certain device preparation procedures. For instance, Zhou *et al*.[26] reported an optimized device fabrication at 30% RH, and we now conclude that at these conditions significant amounts of water is incorporated in the MAPbI layer, which might negatively affect long term stability. Next, current-voltage hysteresis is known to be much less severe in solar cells incorporating PEDOT anodes.[45] PEDOT itself has a strong tendency to take up water[46] and might partially release this water to the MAPbI in the device, which in turn could affect the hysteretic behavior.

The phenomenon of rapid and reversible water embedding into MAPbI observed here is akin to known behaviors of certain metal organic frameworks (MOFs), which are also susceptible for the adsorption of other small gas molecules such as O_2 and N_2.[47,48] We therefore proceeded to investigate the impact of surrounding gas atmospheres on charge transport in controlled environment. Simple lateral devices were prepared by co-evaporating MAPbI on top of Au electrodes (200 µm separation, see SI). Such simple devices as opposed to full solar cells allow us to maximize the MAPbI surface that is exposed to the environment and to avoid possible effects in transport layers.

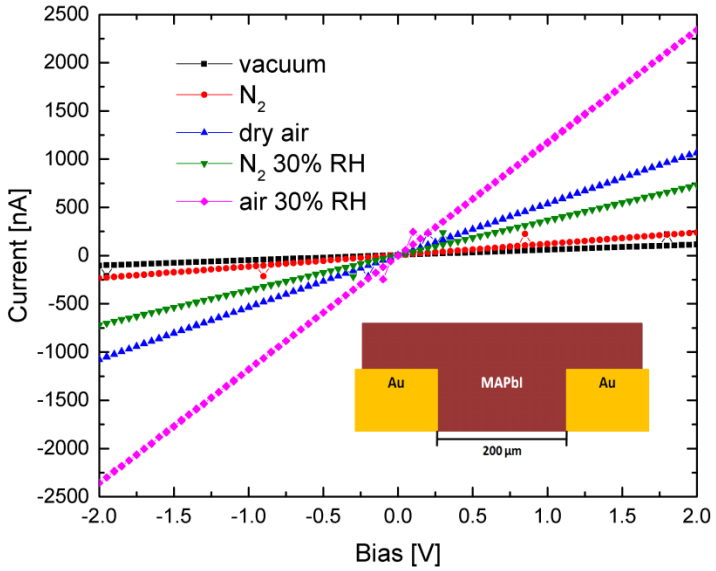

Figure 3. *I*(*V*) measurements under illumination of a lateral MAPbI device in different environments. Film thickness is 350 nm, electrode spacing is 200 µm (see inset). The sample was allowed to equilibrate under each condition in light for at least 3 minutes before the voltage scan. All voltage scans started and ended at 0 V. Minor current increase upon N_2 exposure is attributed to residual water and/or oxygen in the gas system.

We measured current-voltage curves of such lateral devices in the dark and under 1 sun white light illumination with the sample in vacuum, N_2, dry air, N_2 with 30% RH, and air with 30% RH. The sample compartment was pumped down to vacuum between each gas exposure. Figure 3 shows the current under illumination for a 350 nm thick MAPbI layer. The initial *I*(*V*) curve in vacuum shows Ohmic behavior with a current of 110 nA at 2 V applied bias. The moist N_2 (i.e. no oxygen but water) causes a ~6 fold increase of the photocurrent. A similar but somewhat larger effect is observed by sample exposure to dry air (i.e. no water but oxygen) while a combined effect of 30% RH air accounts for an ~20-fold increase of the photocurrent. The photocurrent change is reversible by exposing the samples to vacuum again, with the time required in vacuum depending on the proceeding gas exposure (see SI for photocurrents in vacuum between the gas exposure steps). We studied the effect of air exposure on the photocurrent for a total of 7 devices. We found an increase of the photocurrent upon air exposure in all our devices, but the magnitude of the effect varied from sample to sample (minimum was a three-fold increase, see SI).

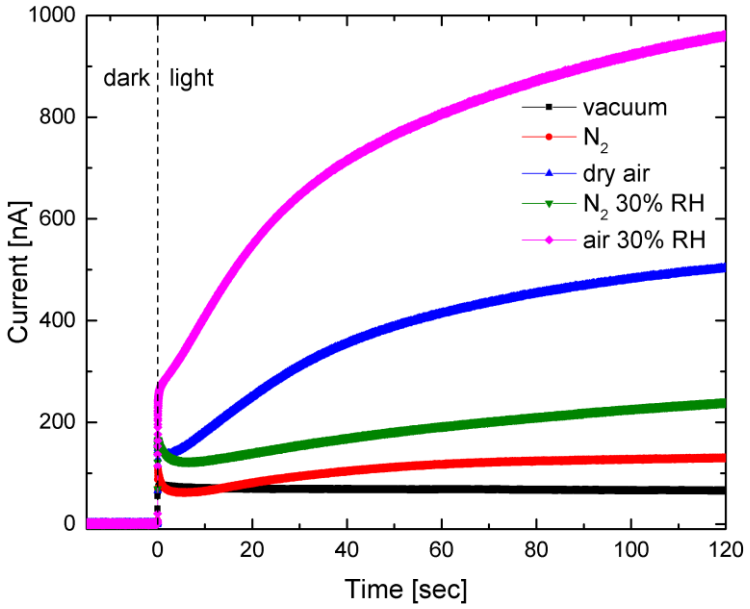

Figure 4. Current vs. time at 1 V applied bias of a lateral MAPbI device in different environments. Film thickness is 350 nm, electrode spacing is 200 µm. The sample is exposed to white light (1 sun) from *t*=0 on.

The mid IR spectra of MAPbI did not show any change when the sample was exposed to oxygen molecules (see Fig. 1b). However, it is reasonable to assume that oxygen molecules can infiltrate MAPbI in a similar way as we observed for water, just as MOFs which are good water absorbers also rapidly absorb oxygen.[47,48] The mechanism for the photocurrent increase upon exposure to ambient environment could be explained via at least two different mechanisms: (i) water/oxygen absorption could affect electronic conductivity via doping or trap state filling and (ii) water/oxygen absorption could increase or trigger ionic conductivity. The fact that the photocurrent in moist air is higher than the sum of photocurrents in dry air and moist N_2 points to a more complex mechanism when both are combined. Measurements of slow photocurrent transients in MAPbI solar cells and lateral devices have

been shown to deliver insights on ionic versus electronic transport.[11,12,49] We therefore monitored the current over time of lateral devices after illumination with white light.

Figure 4 shows such photocurrent transients for the same device as used in Figure 3. An applied bias of 1 V across the 200 µm electrode spacing warrants the regime where field induced effects do not occur.[23,50] The devices were allowed to equilibrate in the dark for at least 3 minutes before we illuminated them with 1 sun white light at t=0. After the rapid increase of current at t=0 due to the photo generated carriers, a slow and weak decrease of photocurrent Is observed for the device in vacuum. We attribute this behavior to the equilibration of charge carrier distribution. Exposure to gas leads to a completely different behavior. First, the photocurrent is immediately higher than in vacuum. Second, we find an additional slow increase of photocurrent, with the timescale in the humid environment seemingly slower than in the oxygen. Whereas the higher instantaneous photocurrent with oxygen and water might well be related to electronic effects such as trap state filling (which is in accordance with the higher photoluminescence yield in ambient conditions, see SI), it is not obvious how this could lead to the slow component in photocurrent increase.

We therefore put forward the notion that water and oxygen uptake have a strong and so far overlooked influence on ionic conductivity in MAPbI. The migration barriers in MAPbI for hydrogen are predicted to be low.[14] The first step towards proton conduction in oxide perovskites is the dissociative absorption of water.[51] The situation in MAPbI is different from oxide perovskites, as hydrogen is ubiquitous in the material even without water. However, it was previously suggested that water could trigger proton conduction.[52] One possible route might be water assisted deprotonation of the methylammonium to methylamine as water is embedded between NH groups and the iodide ions. Similarly, deprotonation in presence of oxygen and light via superoxide has been suggested.[53] Our observation that the increase of conductivity appears only when water or oxygen are combined with light is also in accordance with Egger *et al.*'s[14] notion of a Bourgoin-Corbett mechanism for proton conduction that requires hydrogen species to capture athermal electrons, which are present only under illumination.

Conclusions

In summary, we showed that reversible water infiltration into MAPbI occurs on a time scale of seconds, at relative humidity as low as 10%, and, unlike the formation of the known hydrates, is not accompanied by a change in optical absorbance. This observation suggests that MAPbI is susceptible to inconspicuous infiltration with gas molecules. We present a detailed molecular picture of water embedment based on our quantitative analysis of the IR spectra. We find that for thin MAPbI films in air every other unit cell is occupied with a water molecule. The observed increase of photocurrent under exposure to water and oxygen points to an important contribution of atmospheric gases to ionic conductivity in MAPbI, possibly via hydrogen migration. The presented results have strong implications on intended and unintended moisture and oxygen exposure of MAPbI during and after device fabrication. We believe that this report will spark further studies on the effect of absorbed gases for various types of hybrid perovskite thin films, the dynamics of absorption, and more detailed investigations of the impact on opto-electronic properties in devices.

ASSOCIATED CONTENT

Supporting Information

Further experimental details, absorption spectra in the visible range, further IR spectra, X-ray diffraction measurements, (time-resolved) photoluminescence data.

AUTHOR INFORMATION

Corresponding Authors

[*]pucci@kip.uni-heidelberg.de,

[*]r.lovrincic@tu-braunschweig.de

Author Contributions

[‡] C.M. and T.G. contributed equally to this work.

Notes

The authors declare no competing financial interests.

ACKNOWLEDGMENT

We thank Arava Zohar, Igal Levine, Nir Kedem, and David Cahen (Weizmann Institute, Israel) for helpful discussions. C.M. and M.S. acknowledge support by the Heidelberg Graduate School of Fundamental Physics. A.A.B. is a Royal Society University Research Fellow.

REFERENCES

(1) Mitzi, D. B. Synthesis, Structure, and Properties of Organic-Inorganic Perovskites and Related Materials. In *Progress in Inorganic Chemistry*; Karlin, K. D., Ed.; John Wiley & Sons, Inc., 1999; pp 1–121.

(2) Weber, D. CH 3 NH 3 PBX 3, a Pb (II)-System with Cubic Perovskite Structure. *Z. Für Naturforschung B* **1978**, *33*, 1443.

(3) Kojima, A.; Teshima, K.; Shirai, Y.; Miyasaka, T. Organometal Halide Perovskites as Visible-Light Sensitizers for Photovoltaic Cells. *J. Am. Chem. Soc.* **2009**, *131* (17), 6050–6051.

(4) Lee, M. M.; Teuscher, J.; Miyasaka, T.; Murakami, T. N.; Snaith, H. J. Efficient Hybrid Solar Cells Based on Meso-Superstructured Organometal Halide Perovskites. *Science* **2012**, *338* (6107), 643–647.

(5) Kim, H.-S.; Lee, C.-R.; Im, J.-H.; Lee, K.-B.; Moehl, T.; Marchioro, A.; Moon, S.-J.; Humphry-Baker, R.; Yum, J.-H.; Moser, J. E.; et al. Lead Iodide Perovskite Sensitized All-Solid-State Submicron Thin Film Mesoscopic Solar Cell with Efficiency Exceeding 9%. *Sci. Rep.* **2012**, *2*.

(6) Hodes, G. Perovskite-Based Solar Cells. *Science* **2013**, *342* (6156), 317–318.

(7) Berry, J.; Buonassisi, T.; Egger, D. A.; Hodes, G.; Kronik, L.; Loo, Y.-L.; Lubomirsky, I.; Marder, S. R.; Mastai, Y.; Miller, J. S.; et al. Hybrid Organic–Inorganic Perovskites (HOIPs): Opportunities and Challenges. *Adv. Mater.* **2015**, n/a – n/a.

(8) Frost, J. M.; Butler, K. T.; Walsh, A. Molecular Ferroelectric Contributions to Anomalous Hysteresis in Hybrid Perovskite Solar Cells. *APL Mater.* **2014**, *2* (8), 081506.

(9) Kim, H.-S.; Kim, S. K.; Kim, B. J.; Shin, K.-S.; Gupta, M. K.; Jung, H. S.; Kim, S.-W.; Park, N.-G. Ferroelectric Polarization in CH3NH3PbI3 Perovskite. *J. Phys. Chem. Lett.* **2015**, *6* (9), 1729–1735.

(10) Beilsten-Edmands, J.; Eperon, G. E.; Johnson, R. D.; Snaith, H. J.; Radaelli, P. G. Non-Ferroelectric Nature of the Conductance Hysteresis in CH3NH3PbI3 Perovskite-Based Photovoltaic Devices. *Appl. Phys. Lett.* **2015**, *106* (17), 173502.
(11) Tress, W.; Marinova, N.; Moehl, T.; Zakeeruddin, S. M.; Nazeeruddin, M. K.; Grätzel, M. Understanding the Rate-Dependent J-V Hysteresis, Slow Time Component, and Aging in CH3NH3PbI3 Perovskite Solar Cells: The Role of a Compensated Electric Field. *Energy Environ. Sci.* **2015**.
(12) Eames, C.; Frost, J. M.; Barnes, P. R. F.; O'Regan, B. C.; Walsh, A.; Islam, M. S. Ionic Transport in Hybrid Lead Iodide Perovskite Solar Cells. *Nat. Commun.* **2015**, *6*.
(13) Yuan, Y.; Chae, J.; Shao, Y.; Wang, Q.; Xiao, Z.; Centrone, A.; Huang, J. Photovoltaic Switching Mechanism in Lateral Structure Hybrid Perovskite Solar Cells. *Adv. Energy Mater.* **2015**, n/a – n/a.
(14) Egger, D. A.; Kronik, L.; Rappe, A. M. Theory of Hydrogen Migration in Organic–Inorganic Halide Perovskites. *Angew. Chem. Int. Ed.* **2015**, n/a – n/a.
(15) Frolova, L. A.; Dremova, N. N.; Troshin, P. A. The Chemical Origin of the P-Type and N-Type Doping Effects in the Hybrid Methylammonium–lead Iodide (MAPbI3) Perovskite Solar Cells. *Chem. Commun.* **2015**, *51* (80), 14917–14920.
(16) Edri, E.; Kirmayer, S.; Henning, A.; Mukhopadhyay, S.; Gartsman, K.; Rosenwaks, Y.; Hodes, G.; Cahen, D. Why Lead Methylammonium Tri-IODIDE Perovskite-Based Solar Cells Require a Mesoporous Electron Transporting Scaffold (but Not Necessarily a Hole Conductor). *Nano Lett.* **2014**.
(17) Yun, J. S.; Ho-Baillie, A.; Huang, S.; Woo, S. H.; Heo, Y.; Seidel, J.; Huang, F.; Cheng, Y.-B.; Green, M. A. Benefit of Grain Boundaries in Organic–Inorganic Halide Planar Perovskite Solar Cells. *J. Phys. Chem. Lett.* **2015**, *6* (5), 875–880.
(18) Galisteo-López, J. F.; Anaya, M.; Calvo, M. E.; Míguez, H. Environmental Effects on the Photophysics of Organic–Inorganic Halide Perovskites. *J. Phys. Chem. Lett.* **2015**, 2200–2205.
(19) Eperon, G. E.; Habisreutinger, S. N.; Leijtens, T.; Bruijnaers, B. J.; van Franeker, J. J.; deQuilettes, D. W.; Pathak, S.; Sutton, R. J.; Grancini, G.; Ginger, D. S.; et al. The Importance of Moisture in Hybrid Lead Halide Perovskite Thin Film Fabrication. *ACS Nano* **2015**.
(20) Christians, J. A.; Miranda Herrera, P. A.; Kamat, P. V. Transformation of the Excited State and Photovoltaic Efficiency of CH3NH3PbI3 Perovskite upon Controlled Exposure to Humidified Air. *J. Am. Chem. Soc.* **2015**, *137* (4), 1530–1538.
(21) Tong, C.-J.; Geng, W.; Tang, Z.-K.; Yam, C.-Y.; Fan, X.-L.; Liu, J.; Lau, W.-M.; Liu, L.-M. Uncovering the Veil of the Degradation in Perovskite CH3NH3PbI3 upon Humidity Exposure: A First-Principles Study. *J. Phys. Chem. Lett.* **2015**, 3289–3295.
(22) Koocher, N. Z.; Saldana-Greco, D.; Wang, F.; Liu, S.; Rappe, A. M. Polarization Dependence of Water Adsorption to CH$_3$NH$_3$PbI$_3$ (001) Surfaces. *ArXiv150802415 Cond-Mat* **2015**.
(23) Leijtens, T.; Hoke, E. T.; Grancini, G.; Slotcavage, D. J.; Eperon, G. E.; Ball, J. M.; De Bastiani, M.; Bowring, A. R.; Martino, N.; Wojciechowski, K.; et al. Mapping Electric Field–Induced Switchable Poling and Structural Degradation in Hybrid Lead Halide Perovskite Thin Films. *Adv. Energy Mater.* **2015**, n/a – n/a.
(24) Pathak, S.; Sepe, A.; Sadhanala, A.; Deschler, F.; Haghighirad, A.; Sakai, N.; Goedel, K. C.; Stranks, S. D.; Noel, N.; Price, M.; et al. Atmospheric Influence upon Crystallization and Electronic Disorder and Its Impact on the Photophysical Properties of Organic–Inorganic Perovskite Solar Cells. *ACS Nano* **2015**, *9* (3), 2311–2320.
(25) Wu, C.-G.; Chiang, C.-H.; Tseng, Z.-L.; Nazeeruddin, M. K.; Hagfeldt, A.; Grätzel, M. High Efficiency Stable Inverted Perovskite Solar Cells without Current Hysteresis. *Energy Environ. Sci.* **2015**.
(26) Zhou, H.; Chen, Q.; Li, G.; Luo, S.; Song, T.; Duan, H.-S.; Hong, Z.; You, J.; Liu, Y.; Yang, Y. Interface Engineering of Highly Efficient Perovskite Solar Cells. *Science* **2014**, *345* (6196), 542–546.

(27) Grancini, G.; D'Innocenzo, V.; Dohner, E. R.; Martino, N.; Kandada, A. R. S.; Mosconi, E.; Angelis, F. D.; Karunadasa, H. I.; Hoke, E. T.; Petrozza, A. CH3NH3PbI3 Perovskite Single Crystals: Surface Photophysics and Their Interaction with the Environment. *Chem. Sci.* **2015**.
(28) Leguy, A. M. A.; Hu, Y.; Campoy-Quiles, M.; Alonso, M. I.; Weber, O. J.; Azarhoosh, P.; van Schilfgaarde, M.; Weller, M. T.; Bein, T.; Nelson, J.; et al. Reversible Hydration of CH3NH3PbI3 in Films, Single Crystals, and Solar Cells. *Chem. Mater.* **2015**, *27* (9), 3397–3407.
(29) Halder, A.; Choudhury, D.; Ghosh, S.; Subbiah, A. S.; Sarkar, S. K. Exploring Thermochromic Behavior of Hydrated Hybrid Perovskites in Solar Cells. *J. Phys. Chem. Lett.* **2015**, 3180–3184.
(30) Hailegnaw, B.; Kirmayer, S.; Edri, E.; Hodes, G.; Cahen, D. Rain on Methylammonium Lead Iodide Based Perovskites: Possible Environmental Effects of Perovskite Solar Cells. *J. Phys. Chem. Lett.* **2015**, *6* (9), 1543–1547.
(31) Etgar, L.; Gao, P.; Xue, Z.; Peng, Q.; Chandiran, A. K.; Liu, B.; Nazeeruddin, M. K.; Grätzel, M. Mesoscopic CH3NH3PbI3/TiO2 Heterojunction Solar Cells. *J. Am. Chem. Soc.* **2012**, *134* (42), 17396–17399.
(32) Liu, M.; Johnston, M. B.; Snaith, H. J. Efficient Planar Heterojunction Perovskite Solar Cells by Vapour Deposition. *Nature* **2013**, *501* (7467), 395–398.
(33) Glaser, T.; Müller, C.; Sendner, M.; Krekeler, C.; Semonin, O. E.; Hull, T. D.; Yaffe, O.; Owen, J. S.; Kowalsky, W.; Pucci, A.; et al. Infrared Spectroscopic Study of Vibrational Modes in Methylammonium Lead Halide Perovskites. *J. Phys. Chem. Lett.* **2015**, *6* (15), 2913–2918.
(34) Bakulin, A. A.; Selig, O.; Bakker, H. J.; Rezus, Y. L. A.; Müller, C.; Glaser, T.; Lovrincic, R.; Sun, Z.; Chen, Z.; Walsh, A.; et al. Real-Time Observation of Organic Cation Reorientation in Methylammonium Lead Iodide Perovskites. *J. Phys. Chem. Lett.* **2015**, *6* (18), 3663–3669.
(35) Brivio, F.; Frost, J. M.; Skelton, J. M.; Jackson, A. J.; Weber, O. J.; Weller, M. T.; Goñi, A. R.; Leguy, A. M. A.; Barnes, P. R. F.; Walsh, A. Lattice Dynamics and Vibrational Spectra of the Orthorhombic, Tetragonal, and Cubic Phases of Methylammonium Lead Iodide. *Phys. Rev. B* **2015**, *92* (14), 144308.
(36) Perez Osorio, M. A.; Milot, R. L.; Filip, M. R.; Patel, J. B.; Herz, L. M.; Johnston, M. B.; Giustino, F. Vibrational Properties of the Organic-Inorganic Halide Perovskite CH3NH3PbI3 from Theory and Experiment: Factor Group Analysis, First-Principles Calculations, and Low-Temperature Infrared Spectra. *J. Phys. Chem. C* **2015**.
(37) Cringus, D.; Jansen, T. l C.; Pshenichnikov, M. S.; Wiersma, D. A. Ultrafast Anisotropy Dynamics of Water Molecules Dissolved in Acetonitrile. *J. Chem. Phys.* **2007**, *127* (8), 084507.
(38) Bakulin, A. A.; Cringus, D.; Pieniazek, P. A.; Skinner, J. L.; Jansen, T. L. C.; Pshenichnikov, M. S. Dynamics of Water Confined in Reversed Micelles: Multidimensional Vibrational Spectroscopy Study. *J. Phys. Chem. B* **2013**, *117* (49), 15545–15558.
(39) Walrafen, G. E. Raman Spectral Studies of the Effects of Temperature on Water Structure. *J. Chem. Phys.* **1967**, *47* (1), 114–126.
(40) Mosconi, E.; Azpiroz, J. M.; De Angelis, F. Ab Initio Molecular Dynamics Simulations of Methylammonium Lead Iodide Perovskite Degradation by Water. *Chem. Mater.* **2015**, *27* (13), 4885–4892.
(41) Bonch-Bruevich, V. L. The Optical Properties of Solids. In *The Optical Properties of Solids*; Academic Press: New York, 1966.
(42) Lehmann, A. Theory of Infrared Transmission Spectra of Thin Insulating Films. *Phys. Status Solidi B* **1988**, *148* (1), 401–405.
(43) Mark, P.; Nilsson, L. Structure and Dynamics of the TIP3P, SPC, and SPC/E Water Models at 298 K. *J. Phys. Chem. A* **2001**, *105* (43), 9954–9960.
(44) Stoumpos, C. C.; Malliakas, C. D.; Kanatzidis, M. G. Semiconducting Tin and Lead Iodide Perovskites with Organic Cations: Phase Transitions, High Mobilities, and Near-Infrared Photoluminescent Properties. *Inorg. Chem.* **2013**, *52* (15), 9019–9038.

(45) Bryant, D.; Wheeler, S.; O'Regan, B. C.; Watson, T.; Barnes, P. R. F.; Worsley, D.; Durrant, J. Observable Hysteresis at Low Temperature in "Hysteresis Free" Organic–Inorganic Lead Halide Perovskite Solar Cells. *J. Phys. Chem. Lett.* **2015**, 3190–3194.
(46) Nardes, A. M.; Kemerink, M.; de Kok, M. M.; Vinken, E.; Maturova, K.; Janssen, R. A. J. Conductivity, Work Function, and Environmental Stability of PEDOT:PSS Thin Films Treated with Sorbitol. *Org. Electron.* **2008**, *9* (5), 727–734.
(47) Küsgens, P.; Rose, M.; Senkovska, I.; Fröde, H.; Henschel, A.; Siegle, S.; Kaskel, S. Characterization of Metal-Organic Frameworks by Water Adsorption. *Microporous Mesoporous Mater.* **2009**, *120* (3), 325–330.
(48) Lin, X.; Blake, A. J.; Wilson, C.; Sun, X. Z.; Champness, N. R.; George, M. W.; Hubberstey, P.; Mokaya, R.; Schröder, M. A Porous Framework Polymer Based on a Zinc(II) 4,4'-Bipyridine-2,6,2',6'-Tetracarboxylate: Synthesis, Structure, and "Zeolite-Like" Behaviors. *J. Am. Chem. Soc.* **2006**, *128* (33), 10745–10753.
(49) Gottesman, R.; Haltzi, E.; Gouda, L.; Tirosh, S.; Bouhadana, Y.; Zaban, A.; Mosconi, E.; De Angelis, F. Extremely Slow Photoconductivity Response of CH3NH3PbI3 Perovskites Suggesting Structural Changes under Working Conditions. *J. Phys. Chem. Lett.* **2014**, *5* (15), 2662–2669.
(50) O'Regan, B. C.; Barnes, P. R. F.; Li, X.; Law, C.; Palomares, E.; Marin-Beloqui, J. M. Optoelectronic Studies of Methylammonium Lead Iodide Perovskite Solar Cells with Mesoporous TiO2: Separation of Electronic and Chemical Charge Storage, Understanding Two Recombination Lifetimes, and the Evolution of Band Offsets during J–V Hysteresis. *J. Am. Chem. Soc.* **2015**, *137* (15), 5087–5099.
(51) Kreuer, K. D. Proton-Conducting Oxides. *Annu. Rev. Mater. Res.* **2003**, *33* (1), 333–359.
(52) Frost, J. M.; Butler, K. T.; Brivio, F.; Hendon, C. H.; van Schilfgaarde, M.; Walsh, A. Atomistic Origins of High-Performance in Hybrid Halide Perovskite Solar Cells. *Nano Lett.* **2014**, *14* (5), 2584–2590.
(53) Aristidou, N.; Sanchez-Molina, I.; Chotchuangchutchaval, T.; Brown, M.; Martinez, L.; Rath, T.; Haque, S. A. The Role of Oxygen in the Degradation of Methylammonium Lead Trihalide Perovskite Photoactive Layers. *Angew. Chem. Int. Ed.* **2015**, *54* (28), 8208–8212.